LDA measurements in a non-stenosed and a stenosed model of the carotid artery bifurcation

Please check the document version of this publication:

• A submitted manuscript is the version of the article upon submission and before peer-review. There can be important differences between the submitted version and the official published version of record. People interested in the research are advised to contact the author for the final version of the publication, or visit the DOI to the publisher's website.
• The final author version and the galley proof are versions of the publication after peer review.
• The final published version features the final layout of the paper including the volume, issue and page numbers.

Link to publication

LDA measurements in a non-stenosed and a stenosed model of the carotid artery bifurcation.

D.E.M. Palmen, F.J.H. Gijsen, F.N. van de Vosse, J.D. Janssen and M.E.H. van Dongen *

*Departments of Mechanical Engineering and Physics ***,
Eindhoven University of Technology, P.O.Box 513, 5600 MB Eindhoven, the Netherlands.

ABSTRACT

In order to gain quantitative information of the velocity fields in non-stenosed and stenosed models of the carotid artery bifurcation, Laser Doppler Anemometer (LDA) experiments have been performed. For this purpose a two component backscatter LDA system has been used. The experiments have been conducted in a 1:2.5 enlarged plexiglass model of the carotid artery bifurcation. Both axial and secondary velocities were measured as a function of time at locations of interest. The data were ensemble averaged and analysed in the frequency domain in order to find characteristic flow phenomena. For the frequency analyses, the transfer functions between velocities at specific sites in the bifurcation and the input flow signal have been calculated for both the non-stenosed and the stenosed bifurcation. Both from the results of the velocity fields and the transfer functions, it can be concluded that the main differences between the flow fields in the non-stenosed and the stenosed bifurcation can be found in an area with high velocity and in a shear layer, which is located at the border between a region with low shear rates at the non-divider wall and a region with high shear rates at the divider wall, The values of the transfer functions at these locations seem to be useful for the characterization of the influence of the stenosis.

1. INTRODUCTION

The study of the flow in the carotid artery bifurcation is of great clinical interest with respect to both the genesis and the diagnostics of atherosclerotic disease. This bifurcation consists of a main branch, the common carotid artery, which asymmetrically divides in two branches, the internal carotid artery and the external carotid artery (see also figure 1). In the proximal part of the internal carotid artery a small widening exists, named the carotid sinus (bulb). From clinical practice it is known that the non-divider side of this sinus is very sensitive to the development of atherosclerotic lesions. This local nature of the genesis of the atherosclerotic disease is assumed to be influenced by local characteristics of the flow field. Since hemodynamical aspects play an important role in the diagnostics of atherosclerosis, the flow in models of a normal and a stenosed carotid artery bifurcation can be of great interest. Comparing the results of both cases might lead to parameters of disturbance, that can possibly be used for early detection of the atherosclerotic disease.

Previous studies have dealt with flow patterns in steady flow in three dimensional models of the non-stenosed carotid artery bifurcation. Bharadvaj et al.[1] found a complex flow field in the interna in which secondary flows play an important role. They localized a low-shear region with low (negative) velocities near the non-divider wall which extended with increasing Reynolds number. At the divider side of the carotid sinus a high shear region with high axial velocities was found, separated from the low-shear region by a shear layer. The experiments and computations in steady flow of Rindt et al.[5] confirm these results. A description of the flow behaviour under physiological flow conditions is given by Ku et al.[2]. Hydrogen bubble visualisation showed that during acceleration of the systolic phase a low-shear region was formed at the non-divider side of the sinus. This region extended during the deceleration phase. At the onset of the diastolic phase a small vortex was seen at the edge of the low-shear region near the divider wall. The same authors performed LDA experiments in a three dimensional model of the carotid bifurcation[3]. One of the results from these experiments was the confirmation of the existance of notable velocity disturbances in the shear layer during the deceleration phase and the onset of diastole.

The flow behaviour in mild stenosed carotid artery bifurcations (less than 25% *area* reduction) is less intensively
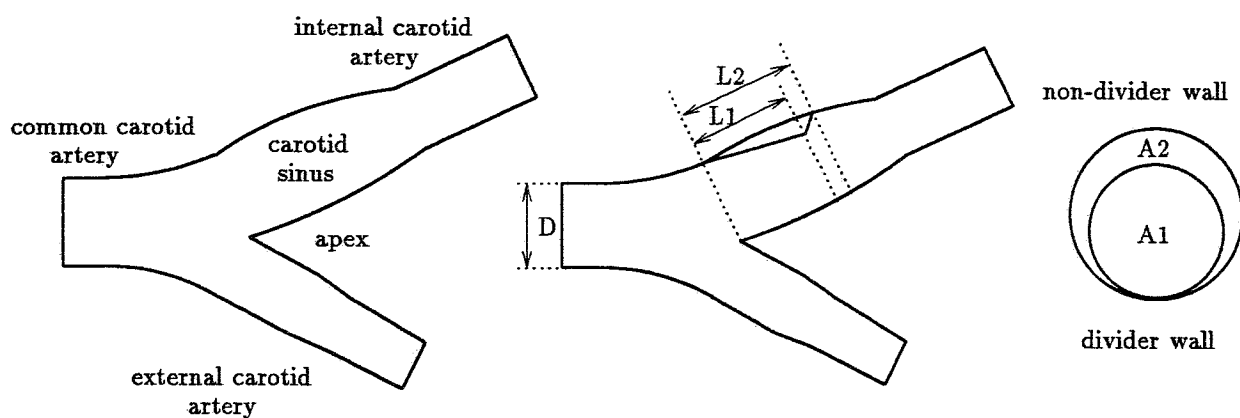
Figure 1: *Geometries of the non-stenosed (left) and the 25% stenosed (center) carotid artery bifurcation in the plane of symmetry and a cross-section of the stenosed carotid sinus (right).*

studied in literature. Van de Vosse *et al.*[6] calculated the velocity field in a two-dimensional geometry of the carotid artery bifurcation in pulsatile flow. They compared 2D axial velocity profiles for a stenosed bifurcation (25% *area* reduction) to the axial velocity profiles of a non-stenosed bifurcation. The influence of the geometry variation on the axial velocity profiles appeared to be relatively small.

To gain an overview of the most important flow phenomena and the locations of interest that are affected by the presence of stenoses, hydrogen bubble visualisation experiments have been performed in plexiglass models of a non-stenosed and a 25% stenosed carotid artery bifurcation by Palmen *et al.*[4]. A physiological range of Reynolds numbers, Womersley parameter and flow ration between the two branches was used. The experiments show that vortex formation may occur in the plane of symmetry at the onset of diastole. This vortex formation is found in a shear layer in the carotid sinus, that is located at the border between a region with low shear rates at the non-divider wall and a region with high shear rates at the divider wall. Comparison of the hydrogen bubble profiles in the 0% and the 25% stenosed models with similar flow conditions shows that the geometric change only slightly influences the flow phenomena. The most striking influences are found in the stability of the shear layer.

In order to quantify the results of the visualisation experiments, LDA experiments have been performed in both the non-stenosed and the stenosed model of the carotid artery bifurcation under identical flow conditions. The LDA experiments also give additional information on the axial and secondary velocities outside the plane of symmetry. The data are ensemble averaged and analysed in the frequency domain in order to find charactaristic frequencies in the flow phenomena.

2. EXPERIMENTAL METHODS

2.1 The fluid circuit

A schematic presentation of the fluid circuit is given in figure 2. The reservoir, containing the measuring fluid, is immersed in a water filled container of constant temperature of 36 °C. A gear pump is used for the generation of the steady flow component (micropump, Verder). The unsteady flow component is generated by a computer controlled plunger pump (superpump, VSI). Before entering the model of the carotid artery bifurcation the fluid passes a buffer and a inlet tube of length $150D$, where D represents the diameter of the common carotid artery. This garantees stable and fully developed flow as the fluid enters the measuring section. Return tubes with taps and flow sensors (transflow 601, Skalar-instruments) transport the fluid back to the reservoir.
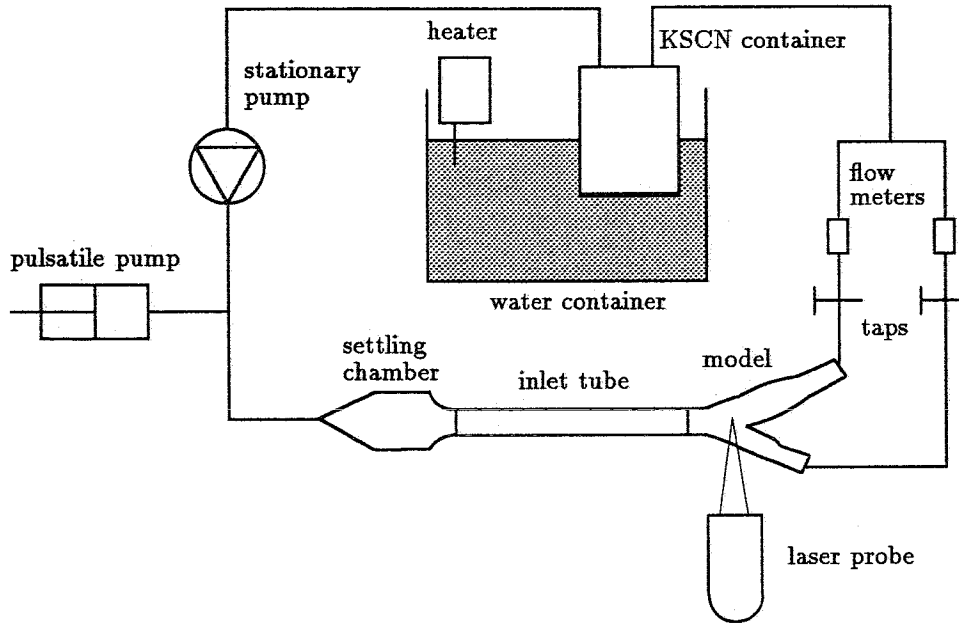
Figure 2: *Schematic presentation of the fluid circuit.*

Two models of the carotid artery bifurcation, one representing a healthy carotid artery bifurcation and another representing a mildly stenosed bifurcation, are used. The geometries and their relevant dimensions are schematically drawn in figure 1. The dimensions of the stenosis are $L_1 = 5D/4$, $L_2 = 11D/8$ and $D = 20mm$. The geometry of the healthy carotid artery bifurcation has been derived from Bharadvaj et al.[1]. The mildly stenosed model has a stenosis in the bulb of the internal carotid artery at the non-divider wall. The stenosis reduces the lumen of the internal carotid artery with 25%. A more extensive description of the models has been given by Palmen et al.[4]. The models have been machined out of plexiglass with an index of refraction equal to 1.491.

To match the index of refraction of the fluid to the one of plexiglass, a concentrated solution of 71 weight percent potassium thiocyanate (KSCN) in water is used as a measuring fluid. The KSCN solution behaves like a Newtonian fluid and the kinematic viscosity at 36 °C is $2.02 \cdot 10^{-6} m^2 s^{-1}$. As a seeding for the LDA experiments aluminium flakes (iriodine 111, Merck) have been added to the KSCN solution in a concentration of about 20 gm^{-3}.

The velocity measurements have been performed by means of a two component fiber optics LDA system in backscatter mode in combination with a Flow Velocity Analyser (58N20, Dantec). A 300 mW Argon-ion laser (5500A, Ion Laser Technology) generates a green laser beam ($\lambda = 514.5nm$) and a blue laser beam ($\lambda = 488.0nm$). With the aid of glass fibers the light is transmitted to the measuring probe. A front lens with a focal length of $80mm$ focusses the laser beams to form one measuring volume with the dimension $50 \times 50 \times 200\mu m$.

2.2 Experimental procedure

The flow pulse consists of a cosine that lasts 20 percent of the period time T, superimposed on a steady flow component. The dimensionless parameters that describe the flow pulse, Re (Reynolds number), α (Womersley parameter) and γ (flow division ratio), are defined as follows

$$Re = \frac{DU}{\nu}, \qquad \alpha = \frac{D}{2}\sqrt{\frac{2\pi}{\nu T}}, \qquad \gamma = \frac{Q_{ECA}}{Q_{CCA}}, \qquad (1)$$

where U represents the cross sectional average of the velocity during peak systole or diastole, D the diameter of common carotid artery, ν the kinematic viscosity of KSCN-solution and Q_{ECA}, Q_{CCA} the flows through the external
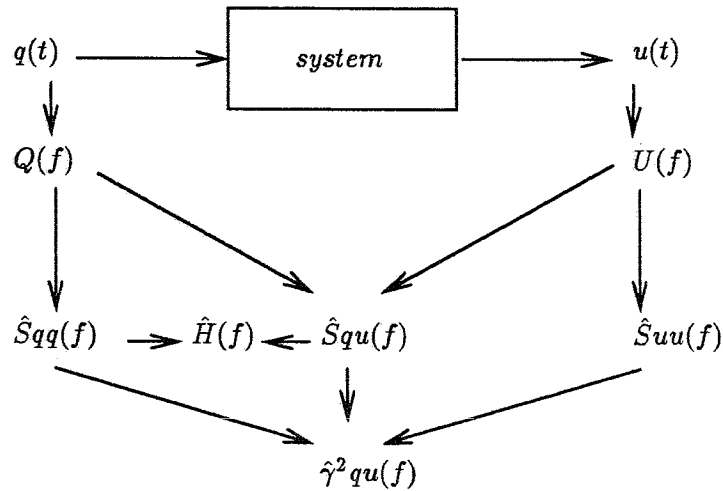
Figure 3: *Data manipulations in the frequency domain.*

and common carotid artery. The experiments have been performed for $Re_{diastole} = 270$, $Re_{systole} = 1000$, and $\alpha = 6$. The mean flow division ratio during a flow pulse was $\gamma = 0.45$.

Velocities have been measured along the centerlines in the plane of symmetry (symmetry axis) and in a plane perpendicular to this plane (horizontal axis). The measurements in the communis (C) are taken along a line at a distance of $3D$ upstream of the apex. In the interna, velocity measurements are taken at 5 sites. Starting at the apex (I_{00}), a new site is defined, moving along the axis of the interna, every $0.5D$ $(I_{05}, I_{10}, I_{15}$ and $I_{20})$. Two velocity components are measured simultaneously. In the communis as well as in the interna, the velocity parallel to the axis of the vessel (axial velocity) and perpendicular to this axis and parallel to the plane of symmetry (secondary velocity) have been measured.

2.3 Data acquisition and data processing

During 16 cycles of 6 seconds, velocities have been measured at each site with an effective data rate of about 30 Hz. To gain a sample record which is equidistant in time, each cycle is divided into 64 intervals and the velocities in these intervals have been averaged, using the residence time of the particle in the measuring volume as a weighting factor. Finally, 8 cycles have been selected to compute the ensemble averaged velocity signal.

The ensemble averaged velocities for the non-stenosed and the 25% stenosed model have been analysed in the frequency domain. As the differences in spectral contents of the non-stenosed and stenosed model are concealed by the spectral contents of the flow pulse, the transfer functions with the mean flow pulse $q(t)$ as an input signal and the local axial velocities $u(t)$ as an output signal have been calculated. In this way the spectral contents of the measured velocities is related to the spectral contents of the common carotid flow pulse. An overview of the data manipulations is represented in figure 3. From the input and output signal $(q(t), u(t))$ a fast Fourier transformation is calculated. With the results of these transformations $(Q(f), U(f))$, the auto- and cross power spectra $(\hat{S}_{qq}(f), \hat{S}_{uu}(f)$ and $\hat{S}_{qu}(f))$ are estimated. Finally, the transfer function $\hat{H}(f)$ and the coherence function $\hat{\gamma}_{qu}^2(f)$ can be estimated as:

$$\hat{H}(f) = \frac{\hat{S}_{qu}(f)}{\hat{S}_{qq}(f)}, \qquad \hat{\gamma}_{qu}^2(f) = \frac{|\hat{S}_{qu}(f)|^2}{\hat{S}_{qq}(f)\hat{S}_{uu}(f)} \qquad (2)$$

The transfer function can be interpreted as the transformation of the harmonics of the q-signal to the harmonics of the u-signal by the system. The coherence function is an indication of the reliability of the estimate of the values of the transfer function.

3. RESULTS

3.1 Velocity measurements

The ensemble averaged signals are presented in three dimensional plots. The axis 'time', 'velocity' and 'position' are made dimensionless by the period of the flow pulse, mean velocity in the communis at end diastole and the local diameter of the vessel. In the interna, 'position = -1' defines the non-divider wall and 'position = +1' is the divider wall. The velocity values at the walls are set to $0\ ms^{-1}$ manually. A short description of the axial velocities in the plane of symmetry at sites C, I_{10} and I_{15} is given below (see also figure 4).

site C : The velocity profiles in the communis are nearly parabolic. Generally, the velocity signals follow the shape of the flow pulse throughout the communis. At near wall sites, small negative velocities can be seen at the onset of diastole. The flow features in the normal and stenosed model are identical.

site I_{10}: At the non-divider wall, after the sytolic peak, a steep velocity gradient during the decelerating phase of the flow pulse is followed by a region with flow reversal. At near wall sites, the region with flow reversal extends till $t/T = 0.6$, gradually decreasing in size as r/R increases. In the shear layer, high velocity during peak systole is followed by a dip in the velocity signal at the onset of diastole. Two oscillations can be seen at $t/T = 0.4$ and $t/T = 0.6$. In the area with high velocity ($r/R = 0.8$) a second peak in the axial velocity develops after the systolic peak at $t/T = 0.3$, followed by a slightly disturbed pattern at the onset of diastole and gradually decreasing velocity during diastole.
The influence of the stenosis involves two aspects. At first, a disturbance of the velocity field with elevated velocities can be seen in the region with flow reversal, starting at $t/T = 0.4$. Secondly the disturbance from the low velocity area extends to the shear layer and seems to interfere with the oscillations in the shear layer. As a result the amplitude of the oscillations as mentioned above enlarges and the frequency diminishes.

site I_{15}: The main flow features as described above can also be found at this site. However, near the non divider wall the region with flow reversal and near zero velocities has decreased in size and only extends till $t/T = 0.4$. For the stenosed bifurcation the disturbance in the area with low velocity is even more pronounced than it was at site I_{10}. It can also be noted that, apart from a more distinct region with flow reversal, no disturbances of the velocity signals are detected just downstream of the stenosis.

Downstream the carotid sinus at site I_{20} convergence of the geometry occurs. As a result the velocity profiles are flatter and the shear layer is hardly visible anymore. The oscillations appear to diminish in amplitude.

3.2 Transfer functions

The data are processed as described in section 2.3. The axial velocity signals in the plane of symmetry at I_{10} and I_{15} serve as the output signals. Both the velocity and the flow signal are scaled between 0 and 1. The transfer functions have been calculated, using 8 cycles with 64 samples. The results at site I_{10} are presented in a three dimensional plot (see figure 5). The dimensionless parameters 'position' and 'harmonic number' have been plotted against the amplitude of the transfer functions and against the coherence function. In the area with low velocity ($r/R = -1$ till $r/R = -0.5$), the transfer functions fluctuate around 1. In this area no significant differences between the normal and the stenosed model at sites I_{10} and I_{15} are found. In the shear layer, the transfer functions at site I_{10} in the normal model show a dip at the 6th harmonic and a gradually increasing value of the transfer functions in the area with high velocity. The stenosed model however, reveals a peak at the 6th harmonic in the shear layer and a local minimum at the 8th harmonic in the area with high velocity. At I_{15}, the general features of the transfer functions are identical to the features at site I_{10}, although they appear at a slightly lower harmonic.

These results are in agreement with the results from the velocity measurements. In the area with low velocity, the shape of the velocity signal resembles the shape of the flow pulse and the expected value of the transfer function is close to 1. In the shear layer and the area with high velocity, the velocity signals deviates from the shape of the flow pulse and differences between the normal and the stenosed model can be found.
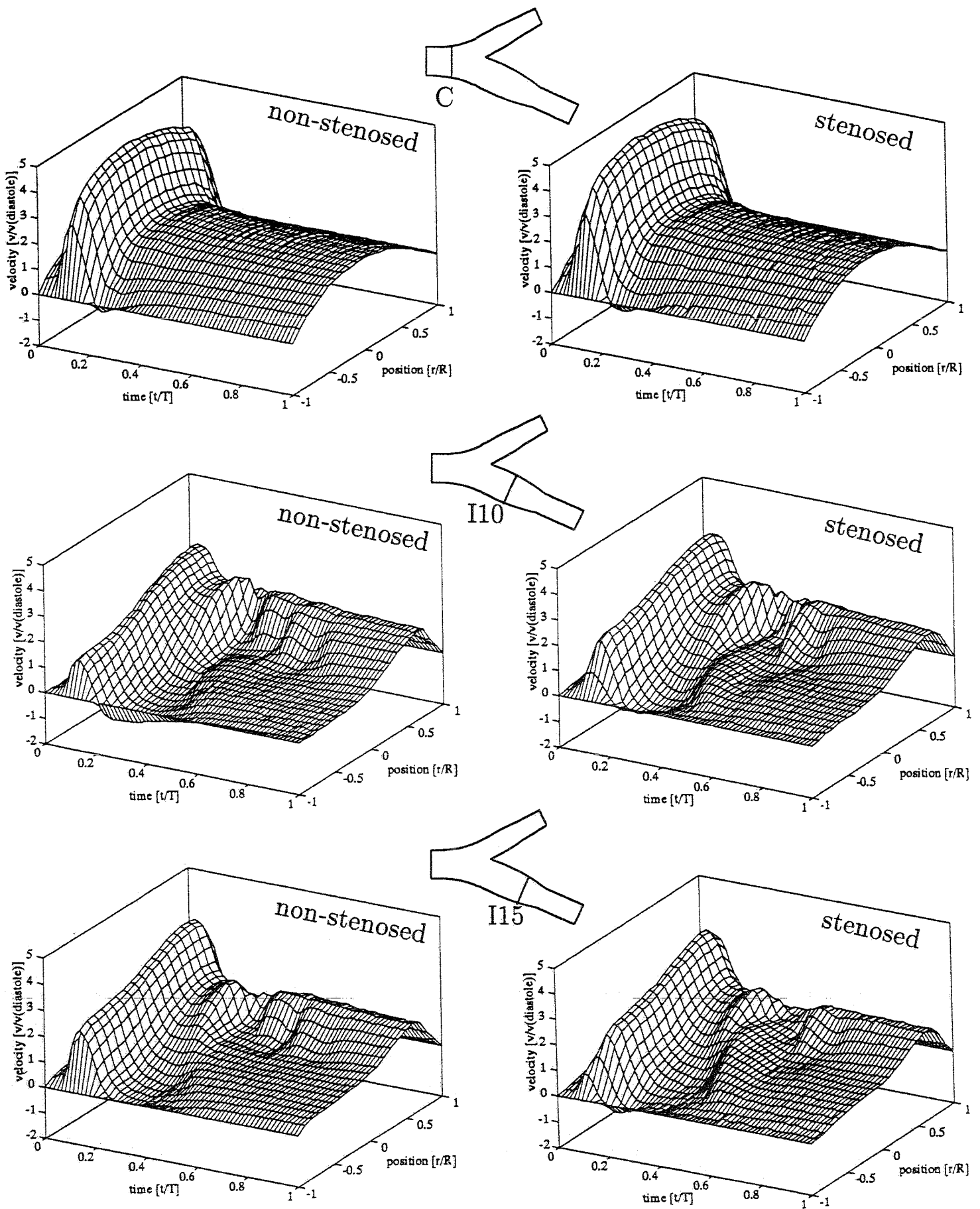
Figure 4: *Axial velocities in the plane of symmetry at sites* C, I_{10} *and* I_{15} *for the non-stenosed (left) and the stenosed bifurcation (right).*
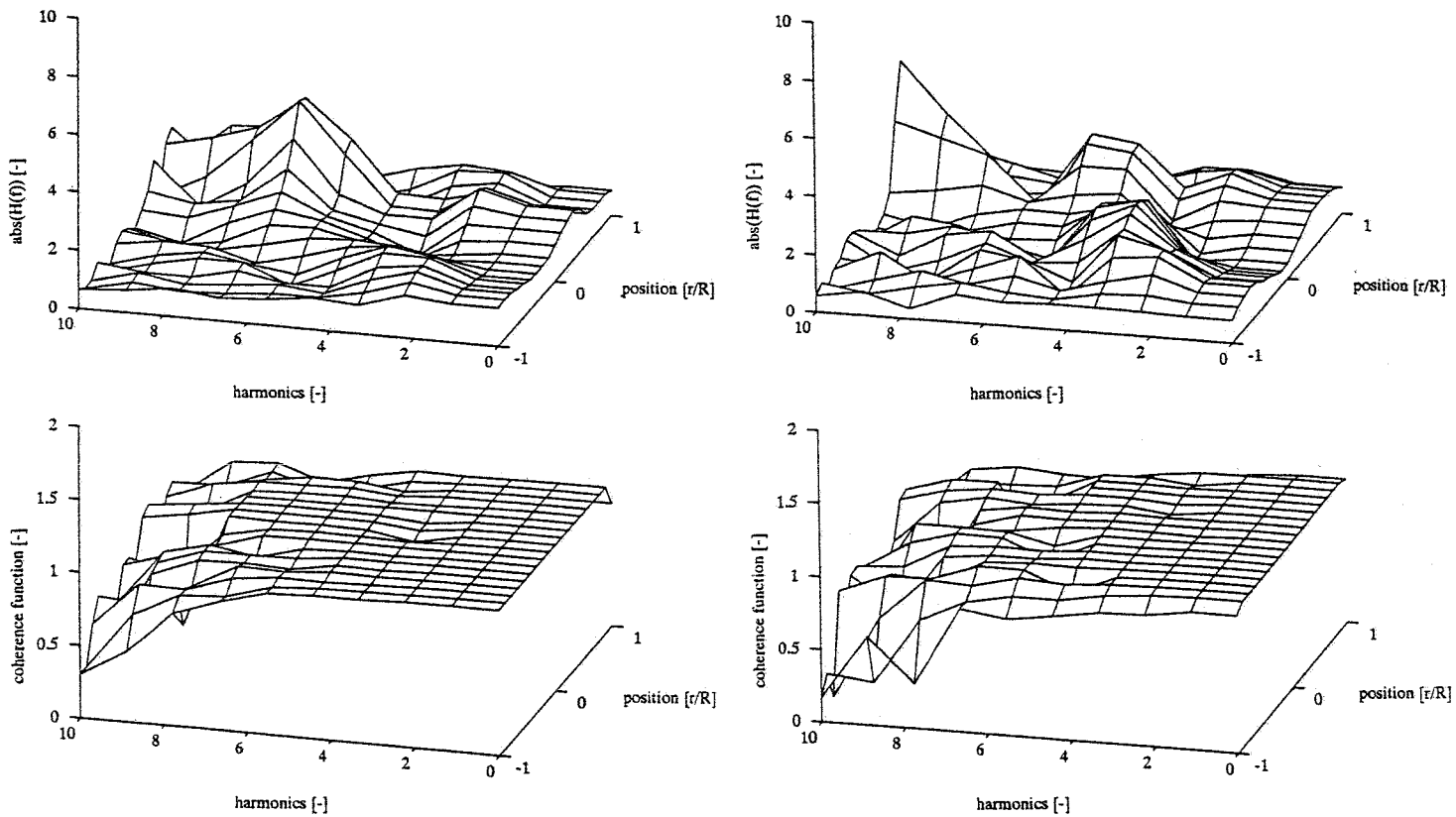
Figure 5: *Transfer function and coherence function at site I_{10} for the non-stenosed (left) and the stenosed bifurcation (right).*

3.3 Error estimation

The errors in the computation of the ensemble averaged velocity signals involve several aspects.

random noise and dimensions measuring volume: The error caused by the noise on the signal and the presence of a velocity gradient in the measuring volume is estimated by the RMS values in stationary flow. It is less than 1% for peak systole and about 1% for diastolic flow.

temporal velocity gradient: Application of the averaging procedure to gain a sample record, which is equidistant in time, can leed to errors due to temporal velocity gradients. For a steep gradient this error can be 3%.

ensemble averaging: Additional errors are introduced by the ensemble averaging procedure in the case that there are no velocity measurements available in a certain time interval. These errors only occur in the low velocity areas and they are assumed to be of the same order as those mentioned above.

According to the errors described above the maximal error can be estimated at 8% during systolic flow and at 3% during diastolic flow.

4. CONCLUSIONS AND DISCUSSION

A LDA method has been applied to obtain quantitative information about the flow field in a normal and stenosed model of the carotid artery bifurcation under physiological flow conditions. Using this method, non-equidistantly spaced velocity sample records can be obtained at specific sites in the bifurcation models. An optimal conversion to an equidistantly spaced sample record has been performed by applying an averaging method, using the residence time of a particle in the measuring volume as a weighing factor. Due to accomplished high spatial and temporal resolution, detailed information about the velocity signals at specific sites has been obtained.

The results of the velocity measurements in the two models compare well to the visualisation studies, performed by Palmen et al.[4]. The differences between the velocity patterns in the two models are small. Emphasis has been put on studying the axial velocity signals in the plane of symmetry and the differences mainly involve two aspects. First, a disturbance with elevated velocities in the area with low velocity appears in the stenosed model. Secondly, oscillations and disturbances in the shear layer and the area with high velocity, which are present in the normal model, are more pronounced and contain different frequencies in the stenosed model. Downstream of the stenosis near the non-divider wall, no disturbance of the velocity signals can be found.

Comparison of the frequency spectra of the velocity signals seems to be an appropriate way to investigate the differences between the flow fields in the two bifurcation models. Computing transfer functions relates the harmonic contents of the flow pulse to the harmonic contents of the velocity signals. The differences between frequency contents of the velocity signals in the two models become more evident. The main discrepancies between the transfer functions in the two models can be found in the shear layer and the area with high velocity. Especially the damping of a higher harmonic in the area with high velocity in the stenosed model is a feature of the transfer function that seems to be connected to the presence of the stenosis. Further research is necessary to determine the influence of the input flow pulse, the geometry of the bifurcation and the shape of the stenosis on the spectral contents of the axial velocity near the shear layer. Numerical computations will be used to investigate the influence of the factors as described above. Combination of these studies finally must give information on the applicability of diagnosing mild stenoses in clinical practice by means of spectral analysis of velocity signals.

5. ACKNOWLEDGEMENTS

6. REFERENCES

1. B.K. Bharadvaj, R.F. Mabon, and D.P. Giddens, 'Steady flow in a model of the human carotid bifurcation. Part I-Flowvisualization, Part II-Laser-Doppler Anemometer measurements,' *J.Biomechanics* Vol. 15, pp. 349-378, 1982ab.

2. D.N. Ku and D.P. Giddens, 'Pulsatile flow in a model carotid bifurcation,' *Arteriosclerosis* Vol. 3, pp. 31-39, 1983.

3. D.N. Ku and D.P. Giddens 'Laser Doppler measurements of pulsatile flow in a model carotid bifurcation,' *J.Biomechanics* Vol. 20, pp. 407-421, 1987.

4. D.E.M. Palmen, F.N. van de Vosse, J.D. Janssen and M.E.H.v. Dongen 'The influence of minor stenoses on the flow in the carotid artery bifurcation,' Submitted to *J.Biomechanics*.

5. C.C.M. Rindt, A.A. van Steenhoven, J.D. Janssen, R.S. Reneman and A. Segal 'A numerical analysis of steady flow in a three-dimensional model of the carotid artery bifurcation,' *J.Biomechanics* Vol. 23, pp. 461-473, 1990.

6. F.N. van de Vosse, A.A. van Steenhoven, J.D. Janssen and R.S. Reneman 'A two-dimensional numerical analysis of unsteady flow in the carotid artery bifurcation,' *Biorheology* Vol. 27, pp. 163-189, 1990.